Journal of Information Hiding and Multimedia Signal Processing ©2009 ISSN 2073-4212
Ubiquitous International Volume **6**, Number **2**, March **2015**

The Algorithm of Estimating the Bubble Size Distribution Characteristics of the Froth Image

Yan-peng Wu[1], Xiao-qi Peng[2*] and Yan-po Song[2]

[1]Department of Information Engineering
Shaoyang University
Shaoyang, Hunan, 422000, China
Central South University
Changsha, Hunan, 410083, China
57844086@qq.com

[2]School of Energy Science and Engineering
Central South University
415 Chien-Kung Road, Kaohsiung, 807, Taiwan
Changsha, Hunan, 410083, China;
*Corresponding author
pengxq126@126.com; songyp@126.com.

Received May, 2014; revised October, 2014

Abstract. *The algorithm of estimating bubble size distribution of the froth image is a key process to realize automation control in related fields. A statistic model of bubble size distribution in the froth image, based on uniform scanning and edge analysis, is established with algorithms of estimating the average deviation angles and average eccentricity as well as estimating the size distribution of round and elliptical bubbles. The simulation results show that the bubbles' transversal width distribution is similar to the size distribution, and the calculation result of estimating the elliptical bubbles' distribution is closer to the actual value than that of the method for estimating round bubbles' distribution.*
Keywords: Edge detection, Froth image, Bubble size distribution, Characteristics recognition.

1. **Introduction.** Foam images are easily seen in such many fields as chemical industry, metallurgical operation, water conservancy, shipping and nuclear industry [1, 2, 3, 4]. The morphological features of the bubble, including number, size, grey value and shapes, are important markers during the industrial manufacturing process. For example, mineral flotation, with either too big or too small bubble size leading to low efficiency of production, needs immediate manual handling [5].

In the idle state, the bubble is almost circular as the pressure around the bubble is approaching balance. In the motion state, the factors such as viscous force, surface tension and outer propulsive force influencing each other, cause the distortion of the bubbles, which usually turn to elliptical ones, and their deviation angles, eccentricity, moving direction, velocity, and surface viscosity are closely related [6]. One practical way is to use image segmentation algorithms such as the watershed or valley edge exploration to edge-segment the bubbles, then calculate respectively the deviation angle, eccentricity and size of every single bubble, and at last figure out the whole characteristic information of the froth image. There is an serious over-segmentation if the froth image is edge-segmented by directly using the watershed method [7]. Yingying Gu and Xiaozhu Lin conducted

an effective segmentation of the adhered slurry bubbles using watershed transformation, and found the stationary physical features such as the number, color and size distribution so as to evaluate, supervise and optimize the flotation process [8]. Rong Zeng proposed an approach of multi-sided regional judgment as regard to the one-bubble-multi-focus problem via the removal of the small basin marker caused by noise, having thus improved the accuracy of segmenting large or medium-sized bubbles using watershed algorithm. To solve the problems such as unsatisfactory image quality and uneven grey values of the bubbles during the mineral flotation [9]. Chunhua Yang applied clustering and high-low-hat transformation to enhance the degree of recognition; and, simultaneously, used area re-structuring and top re-structuring transformation changed into watershed transformation to extract accurate feature markers, thus improving the segmenting effect of the froth image [10]. Though with different improvement, it is still hard to thoroughly eliminate over-segmentation and under-segmentation with more time consumed and errors being relatively big. The other major way to solve the problem is the method based on foam feature determination. Bartolacci extracted foam patterns by using gray level concurrence matrix and wavelet analysis, and applied the least square method to establish an empirical model of the concentrate ore grades [11]. Moolman proposed a method to obtain the average size of the copper ore flotation foam based on fast Fourier transform algorithm [12]. These feature determination algorithms are relatively simple and fast; but the calculation is rough with large errors, thus lacking determination of the essential foam characteristics.

This paper proposes how to establish bubble's transversal distribution model and to estimate the number as well as size distribution of the bubbles in the froth image according to their visually morphological characteristics by scanning the froth image to analyze the bubble edges.

2. **Bubble Edge Scanning of the Foam Image.** Foam image consist of several different sizes of bubbles and their background. Figure 1 shows the aluminum flotation process with image sensor.

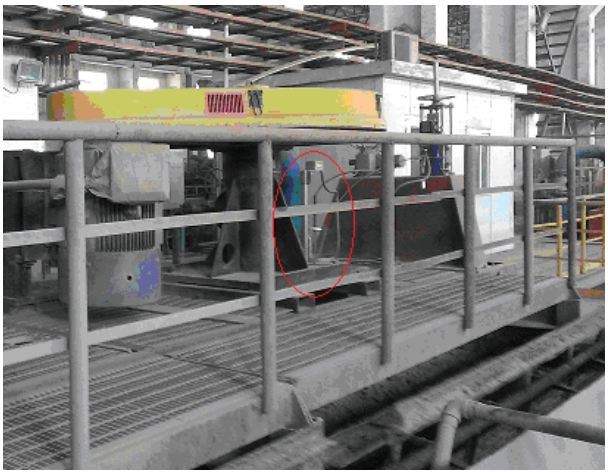

FIGURE 1. Aluminum flotation process with image sensor. A CCD camera is set up at the place marked by red circle.

A foam image consists of a number of bubbles in a background, and Figure 2 shows a typical foam image of aluminum flotation processing. Generally, workers determine condition of aluminum flotation processing by estimating the distribution of bubble size and number [13].

The foam image is scanned between even intervals from a certain angle to produce a number of scanning lines, each of which might penetrate various bubbles. At the same time, a bubble might be penetrated by various scanning lines, with its width in direct proportion to the number of scanning lines. If the scanning interval is smaller than the width of the smallest bubble, then a bubble must be crossed by at least a scanning line according to the smallest drawer principle.

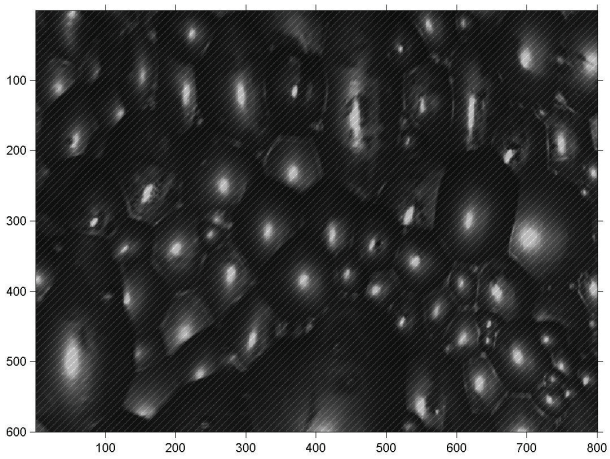

FIGURE 2. A typical foam image with slash lines.

The foam image is scanned between even intervals from a certain angle to produce a number of scanning lines, each of which might penetrate various bubbles. At the same time, a bubble might be penetrated by various scanning lines, with its width in direct proportion to the number of scanning lines. If the scanning interval is smaller than the width of the smallest bubble, then a bubble must be crossed by at least a scanning line according to the smallest drawer principle.

In figure 2, the foam image is graying and evenly bottom-left-to-top- right scanned. The scanning line goes across different bubbles, and the number as well as the widths of bubble serifs can be calculated through bubble edge detection of scanning lines.

3. **Algorithm of Estimating the Bubble Size Distribution of Foam Images.**

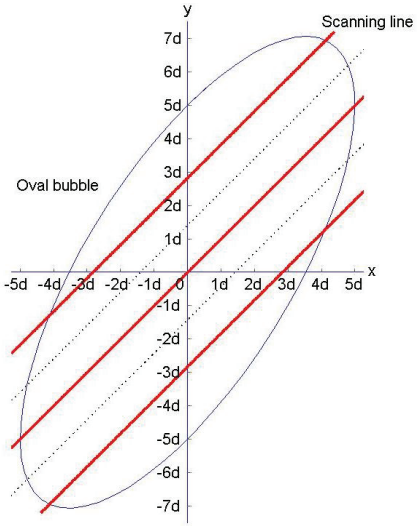

FIGURE 3. Scanning the bubble in direction of 45° with interval of d.

3.1. **Scanning foam images and analysis.** Assuming bubbles in foam image are coaxial and similar to ellipse. Figure 3 shows the elliptical bubbles are uniformly scanned in direction of 45° with interval of d. Mark out scanning lines across bubbles edge, so that number and length of all serifs can be counted.

3.2. **Estimating bubble shape.** Since bubbles are coaxial similar to ellipse, according to assumption, then a super bubble and coaxial and similar to original bubbles can be obtained by merging all bubbles.

Definition 3.1. *Assuming geometric center of super bubble is located at the origin (0, 0), and the general elliptical equations as following:*

$$a \cdot x^2 + b \cdot x \cdot y + c \cdot y^2 - 1 = 0 \tag{1}$$

Providedh_i(i=1, 2, 3, 4) serifs in the 0° direction, 45° direction, 90° direction, 135° direction are scanned, then we get sample points of super bubble edge: $(\frac{h_3 \cdot d}{2}, -\frac{h_3 \cdot d}{2})$, $(\frac{h_4 \cdot d}{2}, -\frac{h_4 \cdot d}{2})$, $(\frac{h_1 \cdot d}{2}, -\frac{h_1 \cdot d}{2})$, $(\frac{h_2 \cdot d}{2}, -\frac{h_2 \cdot d}{2})$. The value of a, b, c are available by least squares dealing [14].

Definition 3.2. *The formula estimating the semi-major axis length, the semi-minor axis length, the angle of deflection, and eccentricity of super bubble as followings:*

$$\Phi = \sqrt{\frac{2}{a + c - \sqrt{(a-c)^2 + b^2}}} \tag{2}$$

$$\Upsilon = \sqrt{\frac{2}{a + c + \sqrt{(a-c)^2 + b^2}}} \tag{3}$$

$$\theta = \frac{1}{2} \cdot \arctan \frac{b}{a - c} \tag{4}$$

$$\omega = \sqrt{1 - \frac{\Upsilon^2}{\Phi^2}} \tag{5}$$

3.3. **Statistics of bubble serif.**

Definition 3.3. *The equation of scanning line of* 0° *direction,* 45° *direction,* 90° *direction,* 135° *direction is as following:*

$$\begin{cases} 0°: & y = (2 \cdot i - 1) \cdot d \\ 45°: & y = x + \frac{\sqrt{2}}{2} \cdot (2 \cdot i - 1) \cdot d \\ 90°: & x = (2 \cdot i - 1) \cdot d \\ 135°: & y = -x - \frac{\sqrt{2}}{2} \cdot (2 \cdot i - 1) \cdot d \end{cases} \tag{6}$$

Definition 3.4. *Suppose the smallest diameter of the recognizable bubble is* $2 \cdot e$.

Definition 3.5. *According to Definition 3.3, the bubbles are classified into m types with the diameter of each type of bubbles being*

$$(i + 2) \cdot e > R_i \geq (i + 1) \cdot e \tag{7}$$

in which i=1, 2, . . . , m.

Definition 3.6. *Similarly, we classify serifs into m types, and the width of every type of serif is:*

$$(i+2)\cdot e > L_i \geq (i+1)\cdot e \tag{8}$$

in which i=1, 2, . . . , m.

Definition 3.7. *Define D_{ij} (i=1, 2, . . . , m; j=1, 2, . . . , i) as effective width of k(k≥j) type serif obtained from scanning i type bubble.*

Definition 3.8. *Define E_{ij}(i=1, 2, . . . , m; j=1, 2, . . . , i) as the quantity expectation of j type serifs across i type bubbles.*

Theorem 3.1. *Set $D_{ij} = 0$ for a convenient calculation. Then*

$$\begin{cases} E_{i1} = \dfrac{D_{i1} - D_{i2}}{d} = \left(\sqrt{(i+1)^2 - 4} - \sqrt{(i+1)^2 - 9}\right)\cdot\dfrac{e}{d} \\ \cdots \\ E_{ij} = \dfrac{D_{i,j-1} - D_{ij}}{d} = \left(\sqrt{(i+1)^2 - j^2} - \sqrt{(i+1)^2 - (j+1)^2}\right)\cdot\dfrac{e}{d} \\ \cdots \\ E_{ii} = \dfrac{D_{i,i-1} - D_{ii}}{d} = \sqrt{2\cdot i + 1}\cdot\dfrac{e}{d} \end{cases} \tag{9}$$

in which i=1, 2, . . . , m; j=1, 2, . . . , i.

3.4. **Calculation of size distribution of circular bubble.** Through uniform scanning, a certain number of bubbles will be segmented by different scanning lines, or on the other way round, every bubble is approximate to the combination of several serifs.

Definition 3.9. *Define the number of bubbles in the foam image G is U_i(i=1, 2, . . . , m).*

Definition 3.10. *Define the number of different types of serifs is V_i(i=1, 2, . . . , m), so,*

$$V_i = \sum_{j=i}^{m} E_{ij}\cdot U_j \tag{10}$$

in which i=1, 2, . . . , m.

Theorem 3.2. *E_{ij} is the known coefficient. We can get the algorithm formula of U_i from formula (5):*

$$\begin{cases} U_m = V_m/E_{mm} \\ U_{m-1} = (V_{m-1} - E_{m,m-1}\cdot U_m)/E_{m-1,m-1} \\ \cdots \\ U_i = (V_i - \sum\limits_{j=i+1}^{m} E_{ij}\cdot U_j)/E_{ii} \\ \cdots \\ U_1 = (V_1 - \sum\limits_{j=2}^{m} E_{2j}\cdot U_j)/E_{11} \end{cases} \tag{11}$$

It's easy to solve formula (11) so in turn we can get the product U_i($i = m$, m-1, . . . , 1) and it is the mere one. The product of $U_i$cannot be negative, or the result would be impractical. Taking into account of the fact that the bubbles are impossible to be standard circular, we should permit an error in the calculation, so that $U_i$can have a non-whole-number product. But the error shouldn't be too big, i.e., the value of U_i can't be too small. Therefore, U_i should be confined to $U_i \geq \lambda$, in which λ refers to the bubble's approximate calculation threshold value in the range [0.7, 0.9].

The process of solving the formula is as follows:

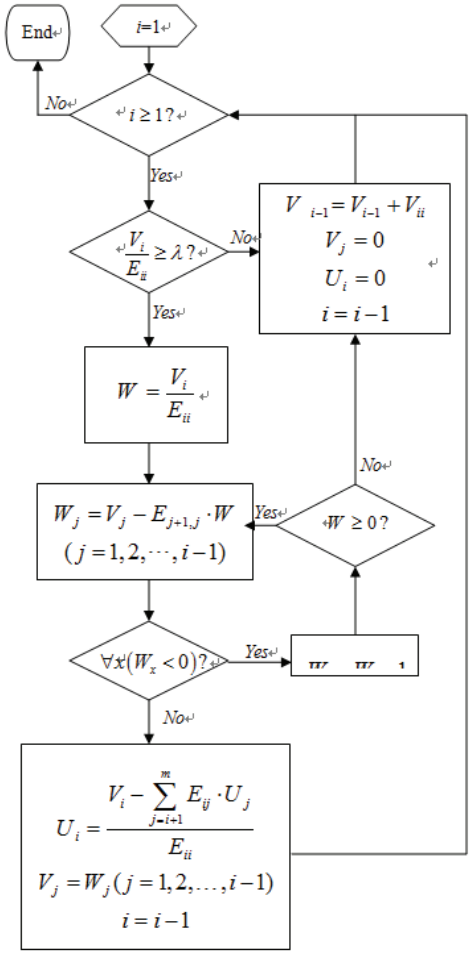

FIGURE 4. The process of calculating the size distribution of circular bubbles.

3.5. **Calculation of size distribution of eclipse bubble.**

Definition 3.11. *If the foam image is evenly scanned from different angles for k times, we calculate the bubble size distribution according to the method suggested in part 3.4 which is respectively* σ_{ij} *(i=1, 2, . . . , k; j=1, 2, . . . , m).*

Definition 3.12. *Assuming the radius of circular bubble with same area as supper bubble be* η*, then*

$$\eta^2 = \Phi \cdot \Upsilon \tag{12}$$

Theorem 3.3. *The estimating formula for calculating the number of bubbles in a foam image as is shown below:*

$$\overline{\sigma} = \frac{1}{k} \cdot \sum_{i=1}^{k} \sum_{j=1}^{m} \sigma_{ij} \tag{13}$$

Theorem 3.4. *The weighted bubble size distribution of the foam image is:*

$$\widetilde{\sigma}_{ij} = \frac{\overline{\sigma}}{k} \cdot \frac{\sum_{i=1}^{k} \sigma_{ij}}{\sum_{j=1}^{m} \sigma_{ij}} \tag{14}$$

4. **Simulated Calculation.** The foam image in Figure 1 is evenly scanned from directions of 0°, 45°, 90°, and 135° with a interval of $d = 10$, and the smallest threshold value of the serif's width is $h = 10$. The edge analysis results are shown in figure 5.

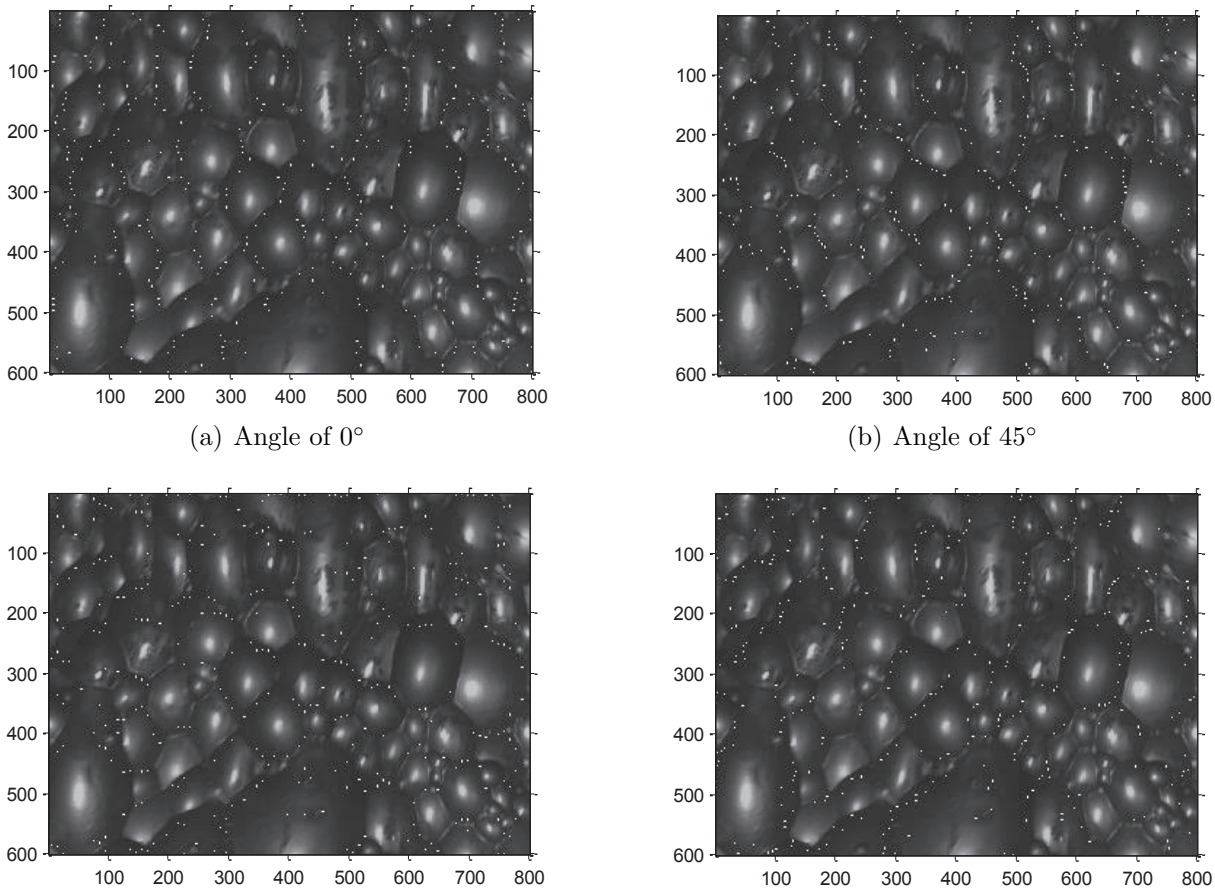

(a) Angle of 0° (b) Angle of 45°

(c) Angle of 90° (d) Angle of 135°

FIGURE 5. Multi-dimension scanning and edge analysis of a foam image, which the white points are the dividing point of serifs.

The number of serifs obtained from sub graph (a), (b), (c), (d) are 386, 401, 460, 418.

With equation (1), (2), (3), (4), (5), we can estimate the fitted elliptic curve as shown in figure 6.

The numbers of bubbles obtained from 4 different scanning angles are respectively 59.3977, 53.7407, 56.6462, 55.7019, and the bubble size distribution is shown in figure 7.

Figure 6 shows that the super bubble is nearly circular, and figure 7 shows that the numbers of transversal lines obtained by scanning from 4 different directions of 0°, 45°, 90° and 135° are basically the same, with a similar transversal distribution. Therefore, the morphological distribution of the bubbles is relatively symmetric.

Figure 6 shows: due to the bubble deformation, the valid scanning width in 0° direction is larger than the diameter of a circle of the equal area; while that in 45° and 135° directions approximate the diameter.

Thus, the estimated numbers of the transversal lines and bubbles in 0° direction are both larger than the average values, and those in 90° direction are both smaller, while those in 45° and 135° directions approximate the average.

Figure 7 shows that the transversal width distribution curves are quite similar to the bubble size distribution curve.

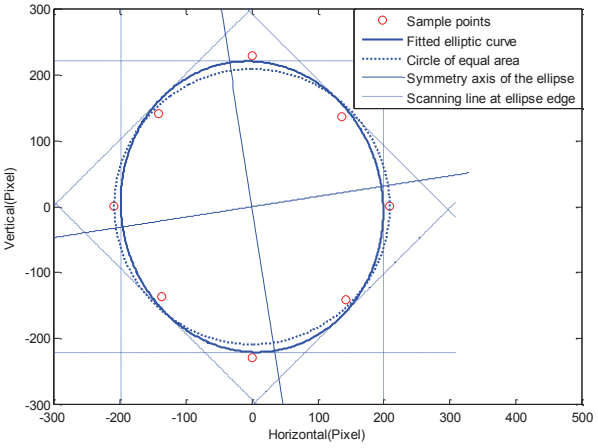

FIGURE 6. Fitted elliptic curve ($\theta = 0.1549$, $\omega = 0.4227$)

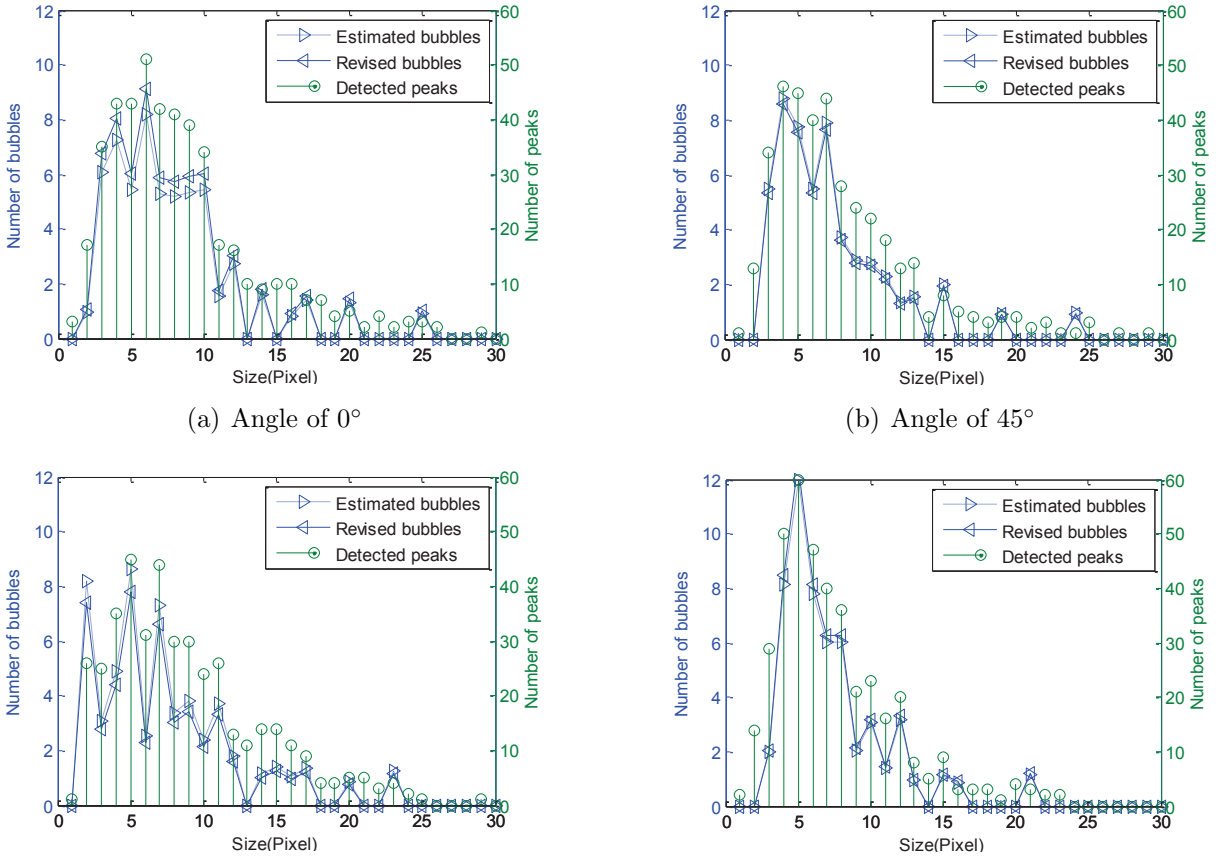

(a) Angle of 0° (b) Angle of 45°

(c) Angle of 90° (d) Angle of 135°

FIGURE 7. Bubble size & serif width distribution

The more large bubbles, the more long transversal lines; the less large bubbles, the less long transversal lines; the more small bubbles, the more short transversal lines; and the less small bubbles, the less short transversal lines. Conversely, the more long transversal lines, the more large bubbles; the more short transversal lines, the more small bubbles. So the transversal width distribution reflects the bubble size distribution, which conforms to actual state.

The bubble size distribution curve modified according to the average deviation angle and eccentricity approximates the transversal width distribution curve, thus being more reliable.

The estimated number of bubbles is 56.8587, and the manually calculated number of bubbles is 58, both of which are basically the same as each other. This indicates that the algorithm proposed in this paper is of high accuracy.

5. **Conclusion.** Usually the bubbles are round or elliptical. If the bubble is round, then the number of times of scanning is always the same from whichever angle. If the bubble is elliptical, then the number of times will be different when scanned from different angles. If the scanning directions are in accordance with the ellipse's long axis, then the number will be the fewest, with the average transversal width being the largest; while the estimated number of bubbles is relatively small, and the average bubble size is relatively big. If the scanning direction is in accordance with the ellipse's short axis, then the number of times of bubbles being scanned will be the largest, with average transversal width being the smallest, while the estimated number of bubbles is relatively large and the average bubble size is relatively small.

The transversal width distribution obtained by multi-dimensional uniform scanning of the froth image is similar to the bubble size distribution.

The average deviation angle and average eccentricity determine different scanning width in different directions as well as different size distribution and number of bubbles.

The estimation algorithm for elliptical bubbles is based on the algorithm for round bubbles, the former algorithm being more accurate than the latter one.

This work is supported by Natural Science Foundation of China (No. 61134006), Natural Science Foundation of China (No. 61273169), Hunan Province Science Foundation of China (No. 14JJ7077) and Fund of Hunan Provincial Education Department of China(No. 13B107).

REFERENCES

[1] W. Zhang and D. Z. Zhu, Bubble Characteristics of Air-water Bubbly Jets in Crossflow, *International Journal of Multiphase Flow*, vol. 55, pp. 156-171, 2013.

[2] N. Zhang and Z. Zong, The effect of rigid-body motions on the whipping response of a ship hull subjected to an underwater bubble, *Journal of Fluids and Structures*, vol. 27, no.8, pp. 1326-1336, 2011.

[3] W. Kracht and J.A. Finch, Effect of foamer on initial bubble shape and velocity, *International Journal of Mineral Processing*, vol. 94, pp. 115-120, 2010.

[4] J. Xu, Timothy A, and Bigelow, Experimental investigation of the effect of stiffness: exposure time and scan direction on the dimension of ultrasound histotripsy lesions, *Ultrasound in medicine & biology*, vol. 37, no. 11, pp. 1865-1873, 2011.

[5] C. Marais and C. Aldrich, Estimation of platinum flotation grades from froth image data, *Minerals Engineering*, vol. 24, no. 5, pp. 433-441, 2011.

[6] Y. Liu, Y. Li, and T. Zhu, Study on modulating shape and velocity of meso-scale bubble using surfactants, *Journal of Xi'an Jiaotong University*, vol. 45, no. 10, pp. 93-97, 2011.

[7] J. Shao and G. Chen, Image segmentation of bubble based on watershed algorithm, *Journal of Xi'an University of Technology*, vol. 27, no. 2, pp. 185-189, 2011.

[8] Y.Y. Gu, X.Z. Lin, and Z.L. Li and C.H. Wang, An image segmentation of flotation froth based on watershed transformation, *Journal of Beijing Institute of Petro-chemical Technology*, vol. 15, no. 1, pp. 61-66, 2007.

[9] R. Zeng, Study of edge detection methods on flotation froth image, *Journal of China University of Mining & Technology*, vol. 31, no. 5, pp. 421-425, 2002.

[10] C.H. Yang and J.Y. Yang, X.M. Mou, K.J. Zhou and W.H. Gui, A segmentation method based on clustering pre-segmentation and high-low scale distance reconstruction for colour froth image, *Journal of Electronics & Information Technology*, vol. 30, no. 6, pp. 1286-1290, 2008.

[11] G. Bartolacci, P. Pelletier Jr., and J. Tessier Jr., C. Duchesne, P.A. Bosse and J. Fournier, Application of numerical image analysis to process diagnosis and physical parameter measurement in mineral processes-Part l: Flotation control based on froth textural characteristics, *Minerals Engineering*, vol. 19, no. 6-8, pp. 734-747, 2006.

[12] D.W. Moolman, C. Aldrich, J.S.J. Van Deventer and W.W. Stange, Digital image processing as a tool for on-line monitoring of froth in flotation plants,*Minerals Engineering*, vol. 7, no. 9, pp. 1149-1164, 1994.

[13] X.Z. Lin, G.Q. Zhao, and Y.Y. Gu, A classification of flotation froth based on geometry, *Proc. of the 2007 IEEE International Conference on Mechatronics and Automation*, pp. 2716-2720, 2007.

[14] B. Yan, B. Wang and Y. Li, Optimal ellipse fitting method based on least-square principle, *Journal of Beijing University of Aeronautics and Astronautics*, vol. 34, no. 3, pp. 295-298, 2008.